Title:

Neurobeachin controls the asymmetric subcellular distribution of electrical synapse proteins

Author names and affiliations:

E. Anne Martin*[1], Jennifer Carlisle Michel[1], Jane Skye Kissinger[1], Fabio A. Echeverry[2], Ya-Ping Lin[3], John O'Brien[3], Alberto E. Pereda[2], Adam C. Miller*[1]

* = corresponding author

[1] Institute of Neuroscience, University of Oregon, United States

[2] Dominick P. Purpura Department of Neuroscience, Albert Einstein College of Medicine, United States

[3] Department of Ophthalmology & Visual Science, University of Texas Health Science Center at Houston, USA[§]

[§] Current address: University of Houston College of Optometry

Abstract

Brain function relies upon the carefully coordinated development of specialized synaptic connections between neurons. The subcellular positioning of synapses and their molecular composition regulate neural computation, forming the fundamental basis of neural circuits. Like chemical synapses, electrical synapses are constructed from an assortment of cell adhesion, scaffolding, and regulatory molecules, as well as channel-forming Connexin proteins, yet little is known about how these molecules localize at specified subcellular compartments of the neuron. Here we investigated the cell biological relationship between the autism- and epilepsy-associated gene Neurobeachin, the gap junction forming neuronal Connexins, and electrical synapse scaffold Zonula Occludens 1 (ZO1). Using the model electrical synapses of the zebrafish Mauthner circuit we found that Neurobeachin localizes to the electrical synapse independent of the ZO1 scaffold and Connexins. By contrast, we show that Neurobeachin functions postsynaptically where it is required for the robust localization of ZO1 and Connexins. We demonstrate that Neurobeachin binds ZO1 but not Connexin proteins. Finally, we find that Neurobeachin is required to restrict postsynaptic electrical synapse proteins to dendritic synapses. Altogether the findings reveal a mechanism for the asymmetric synaptic localization of electrical synapse components providing a basis for the subcellular specialization of neuronal gap junctions.

Introduction

Neuronal synapses can be separated into two classes of fast transmission, chemical and electrical, each of which is required for neural circuit development and function (Pereda, 2014; Jabeen and Thirumalai, 2018). Chemical synapses are well-studied structures with molecularly diverse asymmetrical junctions which are reliant on highly specialized proteins that orchestrate their localization, assembly, and function (O'Rourke et al., 2012; Südhof, 2012). By contrast, electrical synapses are often considered to be simple neuronal gap junction channels composed, in vertebrates, of paired hemichannels of Connexin hexamers that allow for bidirectional flow of ions and other small molecules. Recent work has found that the intracellular scaffold ZO1 is required for electrical synapse structure and function, and a number of cell adhesion molecules, additional intracellular scaffolds, organelles, and cytoskeletal elements have been localized to the electrical synapse (Miller and Pereda, 2017; Nagy et al., 2018; Martin et al., 2020). In addition, electrical synapses can be molecularly asymmetric, with unique protein constituents on each side of the synapse (Marsh et al., 2017; Miller et al., 2017; Alcamí and Pereda, 2019; Martin et al., 2020; Lasseigne et al., 2021). Moreover, the molecular construction of the electrical synapse varies dependent upon the specific neurons coupled and their specific subcellular location. Electrical synapses form between all neuronal compartments with each subcellular coupling yielding different effects on activity. Dendro-dendritic electrical synapses, for example, allow for lateral excitation via the spread of local synaptic potentials between neighboring neurons (Vervaeke et al., 2012). Alternatively, axo-axonic and soma-somatic electrical synapses can promote strong, highly synchronized firing with axo-axonic coupling proposed to contribute to fast ripples such as those aberrantly present in patients with epilepsy (Draguhn et al., 1998; Roopun et al., 2010; Curti et al., 2012; Simon et al., 2014; Alcamí and Pereda, 2019). Thus, the mechanisms by which electrical synapses are established between specific subcellular compartments is critical to understanding neural circuit function.

While the subcellular locations of neuronal gap junctions are critical to function, the mechanisms by which neurons compartmentalize electrical synapse components is not well understood. Recent work in *C. elegans*, which use a different class of

molecules for forming gap junctions called Innexins, identified a cAMP-dependent signaling pathway regulating the trafficking of Innexins to distal synaptic sites, yet this pathway was dispensable for somatic electrical synapses (Palumbos et al., 2021). The findings support the notion of differential regulatory mechanisms in trafficking electrical synapse proteins to distinct subcellular locations, but it is not clear if vertebrate Connexins share related pathways. For chemical synapses, the mechanisms controlling the polarized distribution of synaptic proteins to axons and dendrites are well understood and require the coordination of motor proteins, the cytoskeleton, and numerous adaptors and regulators to ensure the fidelity of compartmentalized delivery (Ou et al., 2010; Easley-Neal et al., 2013; Maeder et al., 2014; Mignogna and D'Adamo, 2017). Whether there are distinct, or shared, mechanisms to guide the polarized transport of electrical synapse proteins remains unknown. The formation of electrical and chemical synapses are generally thought to be cell biologically and biochemically distinct processes. Yet in recent years, molecules have emerged that suggest links between the development and function of these structures (Pereda, 2014; Miller et al., 2015; Jabeen and Thirumalai, 2018; Martin et al., 2020). One of these proteins, Neurobeachin, was recently shown to be required for both electrical and chemical synapse development (Miller et al., 2015). Neurobeachin is a large (~330 kDa) protein that is highly conserved in vertebrates and contains various protein-binding domains including a BEACH domain, AKAP domain, and multiple WD40 domains (Wang et al., 2000). More than 20 *de novo* variants of Neurobeachin have been identified in patients with autism, intellectual disability, and epilepsy, with these mutations occurring across many of the recognized domains (De Rubeis et al., 2014; Iossifov et al., 2014; Bowling et al., 2017; Mulhern et al., 2018). Past work suggests Neurobeachin regulates membrane protein trafficking of chemical synapse scaffolding proteins such as SAP102 and PSD95 (Wang et al., 2000; Medrihan et al., 2009; Niesmann et al., 2011; Nair et al., 2013; Farzana et al., 2016), but its role in electrical synapse development is unknown.

Here we explore the contributions of Neurobeachin to electrical synapse formation and examine its biochemical and cell biological functions. We used the stereotyped and identifiable synaptic contacts of the Mauthner cell of larval zebrafish as they are accessible to genetic, biochemical, and cell biological analysis. We show that

Neurobeachin is localized to the electrical synapse where it functions postsynaptically to robustly localize the electrical synapse scaffold ZO1 and neuronal Connexins. We find that Neurobeachin interacts with ZO1 but not the Connexin proteins, supporting a hierarchical model of electrical synapse formation. Further, we find that Neurobeachin functions to restrict postsynaptic electrical synapse proteins to the dendrite, such that in its absence postsynaptic proteins are inappropriately localized and stabilized at presynaptic locations in the axon. These results reveal an expanded understanding of electrical synapse complexity and hierarchical interactions in building neuronal gap junctions. Further, these findings provide novel insight into the mechanisms of the compartmentalized localization of electrical synapse formation, providing a basis for the subcellular specificity of electrical synapse formation and function.

Results

Neurobeachin localizes to electrical synapses independent of ZO1 and Connexins

To investigate how Neurobeachin regulates electrical synapse development we used the zebrafish Mauthner cell circuit, which controls a fast escape response using a combination of electrical and chemical synapses (Kimmel et al., 1981; Liu and Fetcho, 1999; Sillar, 2009). This circuit is composed of two Mauthner cells per fish that receive sensory input from several modalities, including the auditory system, and output onto motorneurons and interneurons in the spinal cord, including Commissural Local (CoLo) interneurons. Electrical synapses are prominent throughout the circuit, including at mixed electrical/glutamatergic inputs from auditory afferents onto the lateral Mauthner dendrite, called club ending (CE) synapses (Yao et al., 2014). Additionally, the Mauthner cell uses electrical synapses at outputs between its axon and CoLos, called M/CoLo synapses (Figure 1A,B). These M/CoLo synapses repeat down the length of the spinal cord, with CoLo being present as a single cell in each of the hemisegments (Satou et al., 2009). The CE and M/CoLo electrical synapses are molecularly asymmetric, composed of presynaptic Connexin 35.5 (Cx35.5) hemichannels that pair with postsynaptic Cx34.1 hemichannels (Miller et al., 2017a). In addition, the electrical synapse scaffold ZO1b localizes exclusively postsynaptically where it binds Cx34.1 (Figure 1B) (Marsh et al., 2017; Lasseigne et al., 2021). At the CE synapses, the

Mauthner cell is the postsynaptic partner and uses ZO1b and Cx34.1 to build electrical synapses, while at the M/CoLo synapses, the Mauthner cell is presynaptic and uses Cx35.5 (Figure 1B). The asymmetry of the Mauthner cell electrical synapses highlights the cell biological requirement of the neuron to deliver unique electrical synaptic proteins to distinct neuronal compartments.

In electron microscopic analyses of rat cerebellar neurons, Neurobeachin localizes to the trans side of the Golgi, on tubulovesicular vesicles in dendrites, and at the postsynapse of glutamatergic chemical synapses (Wang et al., 2000). Thus, we first chose to examine Neurobeachin localization at electrical synapses of the Mauthner cell circuit. At 5 days post fertilization (dpf), we observe Neurobeachin localization in the Mauthner cell soma, but little to no colocalization with electrical synapse proteins in this compartment (Figure 1C). At the CE synapses on the lateral dendrite, we see Neurobeachin localization at distinct foci adjacent to the electrical synapse proteins ZO1b and Cx34.1, as well as a diffuse staining colocalized across the extent of the observed gap junction staining (Figure 1D). Rarely, we see Neurobeachin staining at M/CoLo synapses along the axon, but not in the axon outside of synapses (Figure 1E,F). Neurobeachin staining is eliminated in Neurobeachin mutants supporting the specificity of the antibody (Supplemental Figure 1A-D). Overall, we conclude that Neurobeachin can localize to electrical synapses.

Electrical synapse structure and function is built hierarchically wherein ZO1b is required for Connexin localization, but ZO1b largely localizes independently of the Connexins (Lasseigne et al., 2021). We therefore sought to determine if localization of Neurobeachin to the electrical synapse was dependent on ZO1b or Connexins. We examined *tjp1b/ZO1b*-/- (Marsh et al., 2017) and *gjd1a/Cx34.1-/-* (Miller et al., 2017) mutant fish and found that Neurobeachin localizes to mutant electrical synapses in a manner similar to their wildtype siblings (Figure 1G-L). We conclude that Neurobeachin localizes to the electrical synapse independent of ZO1b and Connexins.

Neurobeachin is required for the localization of pre- and post-synaptic electrical synapse proteins

Given Neurobeachin's localization, we next asked whether it was required for the localization of both presynaptic Cx35.5 and postsynaptic ZO1b and Cx34.1 (Figure 2A-F). We first examined 5 dpf wildtype and *nbeaa-/-* mutant fish (Miller et al., 2015) for Cx35.5 and Cx34.1 localization at CE (Figure 2A,B,G) and M/CoLo synapses (Figure 2D,E,H). In *nbeaa-/-* mutants, we observed similar decreases of both pre- and post-synaptic Connexin proteins at the synapses. Using a transgenic line that marks endogenous ZO1b with a V5 epitope (Lasseigne et al., 2021), we examined 5 dpf wildtype and *nbeaa-/-* mutant fish for ZO1b at CE (Figure 2C,G) and M/CoLo synapses (Figure 2F,H). We observe a similar loss of ZO1b at the electrical synapse in *nbeaa-/-* mutant fish. The diminished synaptic localization is likely not due to an overall loss of electrical synapse proteins as western blots confirm similar Cx35.5, Cx34.1, and ZO1b protein levels are present in both wildtype and *nbeaa-/-* mutant fish (Supplemental Figure 2). We conclude that Neurobeachin is required for the synaptic localization of pre-synaptic Cx35.5 and post-synaptic ZO1b/Cx34.1.

Neurobeachin binds the electrical synapse scaffold ZO1b but not the Connexins

Neurobeachin is thought to orchestrate the delivery of receptors to the glutamatergic chemical synapse through binding with chemical synapse scaffolds such as MAGUK family members PSD95 and SAP102 (Lauks et al., 2012; Farzana et al., 2016). The electrical synapse scaffold ZO1b is also a member of the MAGUK family of intracellular scaffolds. Neurobeachin has also been shown to bind to the glycine receptor beta subunit (del Pino et al., 2011). Thus, we next questioned if Neurobeachin could regulate electrical synapse development via interaction with ZO1b or Connexin. We first co-transfected mVenus-tagged C-terminal Neurobeachin with ZO1b in HEK293 cells and performed coimmunoprecipitation assays (Figure 3A). We find that the C-terminal fragment of Neurobeachin pulls down with ZO1b (Figure 3B). We next tested if the pre or postsynaptic Connexins could bind Neurobeachin. We co-transfected each Connexin with N-terminal and C-terminal Neurobeachin and find no evidence of pull down in immunoprecipitates (Figure 3C,D). We conclude that Neurobeachin binds the postsynaptic electrical synapse scaffold ZO1b.

Neurobeachin is required postsynaptically for pre- and postsynaptic electrical synapse protein localization

Observing that Neurobeachin binds ZO1b, which functions postsynaptically (Lasseigne et al., 2021), we next wanted to examine electrical synapse protein localization when Neurobeachin is removed exclusively from the Mauthner cell. To achieve this we generated chimeric animals via blastula transplantation (Kemp et al., 2009)(Figure 4A) and we first examined the localization of ZO1b within the Mauthner cell. Donor embryos were *Et(Tol-056:GFP)*; *Pt(V5-ZO1b^{b1406})* double transgenics, which label Mauthner cells with GFP and ZO1b protein with a V5 epitope tag. The double transgenic donor embryos were either *nbeaa+/+* (WT control) or *nbeaa-/-* mutant. All host embryos were non-transgenic wildtypes – thus the observed V5-ZO1b staining is associated exclusively with the GFP+ Mauthner donor cells. Examination of V5-ZO1b at the dendritic CE synapses in *nbeaa-/-* Mauthner cells exhibited reduced V5 staining compared to wildtype transplants (Figure 4B). These data reveal that Neurobeachin functions postsynaptically to localize ZO1. In similar experiments, we next examined the Connexins and used *nbeaa+/+* or *nbeaa-/-* mutant animals with the *Tg(Cx34.1-GFP^{AE37})* transgenic line that labels Cx34.1 with GFP as the donor. In *nbeaa-/-* transplanted Mauthner neurons, we observe that postsynaptic Cx34.1-GFP, as well as presynaptic Cx35.5, is reduced at dendritic CEs compared to wildtype transplants (Figure 4C). These data show that the removal of Neurobeachin exclusively from the postsynaptic neuron affects the localization Connexins on both sides of the electrical synapse. Taken together, these data support an expanded electrical synapse hierarchy, with Neurobeachin independently localizing to neuronal gap junctions where it binds ZO1b and is required postsynaptically for the robust localization of both pre- and postsynaptic electrical synapse proteins.

Neurobeachin is required to restrict postsynaptic electrical synapse proteins to the dendritic compartment

We next took advantage of the fact that the Mauthner cell is both a postsynaptic partner at the CEs as well as the presynaptic partner at the M/CoLo synapses. This configuration, in conjunction with the chimeric transplant experiments, allows us to

visualize the compartmentalized localization of components of the electrical synapse. In wildtype transplants, the V5-tagged ZO1b is exclusively localized at CE synapses and is not present at M/CoLo synapses (Figure 4B,D, left panels). Thus, within the Mauthner cell, ZO1b is compartmentalized exclusively postsynaptically to the dendritic synapses and excluded from localizing presynaptically within the axon. Surprisingly, in *nbeaa-/-* transplanted Mauthner cells, we observed localization of V5-ZO1b presynaptically at M/CoLo synapses (Figure 4D, right panels, quantified in F). The Mauthner cell axon extends the length of the spinal cord (Figure 1A), and it makes *en passant* electrical synapses with CoLo neurons found in each hemi-segment. The mislocalized V5-ZO1b appears strongly at M/CoLo synapses found in the anterior half of the spinal cord, and diminishes at synapses found posteriorly (Figure 4G). We conclude that Neurobeachin is required to restrict ZO1b localization to the dendritic compartment and prevent it from localizing at axonal sites.

ZO1b is necessary for connexin localization to the synapse and binds Cx34.1 *in vivo*, but not Cx35.5 (Lasseigne et al., 2021). Therefore, we hypothesized that Cx34.1 would also mislocalize to the presynapse if Neurobeachin was removed from the Mauthner cell. In wildtype transplants, Cx34.1-GFP is exclusively found compartmentalized to the CEs and not at M/CoLo synapses (Figure 4C,E, left panels). By contrast, we observe that *nbeaa-/-* Mauthner neurons mislocalize Cx34.1-presynaptically at axonal M/CoLo synapses (Figure 4E, right panels, quantified in H). In addition, analogous to our V5-ZO1b transplant experiments, this mislocalization of Cx34.1 appears strongly at anterior M/CoLo synapses and diminishes postereriorly (Figure 4I). Taken together, we find that in the absence of Neurobeachin, both the postsynaptic electrical synapse scaffold, ZO1b, and the postsynaptic Connexin, Cx34.1, are reduced at the dendritic CEs postsynapses, and instead mislocalize to the axonal M/CoLo presynapses.

We considered that neuronal polarity could be disrupted in Neurobeachin mutants, and consequently, all compartment-specific transport could be affected. To address this possibility, we first compared the neuronal morphology of wildtype and *nbeaa-/-* fish and observed that the Mauthner cell dendrites and axons form normally and do not show altered targeting or gross morphological defects (Supplemental Figure

4A). Secondly, we examined the subcellular distribution of the Golgi apparatus in the Mauthner cell of wildtype and *nbeaa-/-* animals. The positioning of the Golgi apparatus, and its interaction with cytoskeletal elements, can be influential in the establishment of neuronal polarity (Yadav and Linstedt, 2011; Ravichandran et al., 2020). We observed extensive Golgi staining (GM130) within the Mauthner soma, with an asymmetrically biased localization towards the axon; this distribution was not altered in *nbeaa-/-* mutants (Supplemental Figure 4B). In addition, we noticed a high degree of colocalization of Neurobeachin with the Golgi, similar to what has been observed in rodents (Wang et al., 2000; Nair et al., 2013). Finally, we examined whether presynaptic Cx35.5 was mislocalized in Neurobeachin mutants. We used CRISPR to V5-tag endogenous Cx35.5 protein and examined injected mosaic F0 animals ("CRISPants") for the localization of Cx35.5-V5 in wildtype and *nbeaa-/-* Mauthner cells. In wildtype, CRISPant animals, we identified animals in which no Cx35.5-V5 staining was observed at CE synapses, but all M/CoLo synapses have V5 staining (Supplementary Figure 4C). This pattern is expected when only the Mauthner cell is expressing Cx35.5-V5 as it is presynaptic to all M/CoLo synapses in the spinal cord, but uses Cx34.1 at its dendritic synapses. In *nbeaa-/-* CRISPants, axonal Cx35.5-V5 is present at all M/CoLo synapses, however the amount localized is reduced – this is expected given that *nbeaa-/-* mutants have diminished presynaptic localization (see Figure 2). Critically, in such animals, no Cx35.5-V5 staining is observed at CE synapses (Supplementary Figure 4D). Thus, we conclude that Neurobeachin functions specifically to constrain dendritically localized synaptic components to their appropriate compartment, thereby supporting the subcellular specificity of electrical synapse formation (Figure 4J).

Discussion

In this paper we have made biochemical and cell biological insights that change our understanding of the development of electrical synapse molecular organization. First, we have expanded our knowledge of the hierarchy and construction of the molecular components of the electrical synapse, adding further support to the notion that electrical synapses, like chemical synapses, are molecularly complex cell-cell contacts. We find that Neurobeachin localizes to the electrical synapse independent of ZO1b or

Connexins, yet it itself is necessary for these proteins to robustly localize to the developing synapse. Furthermore, we have identified a biochemical connection between Neurobeachin and ZO1b, and previous work found that ZO1b in turn binds Cx34.1 (Lasseigne et al., 2021). Thus, our emerging model is that Neurobeachin sits at the top of an electrical synapse hierarchy, directing ZO1b to the synapse, which in turn brings in the Connexin to build the neuronal gap junction. We further show that Neurobeachin functions postsynaptically in building the electrical synapse, and so why are the presynaptic Cx35.5 proteins affected? We have observed that the removal of the postsynaptic Cx34.1 from the synapse results in a decrease in presynaptic Cx35.5 localization (Miller et al., 2017). Thus, we hypothesize that the decreased presynaptic Cx35.5 observed in *nbeaa-/-* animals is most likely due to the diminished postsynaptic Cx34.1 localization. Therefore, we have established that Neurobeachin is directly required for the compartmentalized synaptic localization of postsynaptic electrical synapse proteins. Considering these results, we propose a model in which Neurobeachin is likely necessary for the trafficking and stabilization of postsynaptic proteins to the electrical synapse (Figure 4J).

Intriguingly, the loss of Neurobeachin results in the loss of asymmetry at the M/CoLo electrical synapses. Rather than specific postsynaptic proteins targeting the dendrite, we now have all pre and postsynaptic proteins accumulating at the axonal presynapse. Molecular asymmetry between the electrical pre and postsynapse can determine the functional properties of the synapse, for instance to allow for electrical rectification (Rash et al., 2013). In addition, past research shows the localization of electrical synapses to different subcellular compartments to be of critical importance for neuronal function (Alcamí and Pereda, 2019). Here, we have identified a mechanism by which Neurobeachin appears to direct electrical synapse components to a specific subcellular compartment, the dendrite. However, within the Mauthner cell, we are unable to observe Connexin and ZO1b proteins while they are being trafficked to their synaptic sites. Instead, we can only view these proteins once they have accumulated at synaptic structures. Therefore, we cannot exclude the possibility that electrical synapse proteins are trafficked into each compartment and are only stabilized at the correct putative synapse site by Neurobeachin. Never the less, our results clearly demonstrate

that Neurobeachin is required to restrict the postsynaptic ZO1b and Cx34.1 to their normal dendritic synaptic locations. Future technical improvements in detection and imaging will be required to assess the trafficking pathways taken by these, and other, electrical synapse proteins. Neurobeachin contains an A-Kinase Anchoring Protein (AKAP) domain which could promote the formation of a synaptic PKA signaling complex to phosphorylate electrical synapse proteins upon cAMP stimulation (Wang et al., 2000; Autenrieth et al., 2016). Phosphorylation can alter gap junction processes in a wide range of ways from trafficking, to assembly and degradation, to channel function (Lampe and Lau, 2000). Given the findings in C. elegans that cAMP signaling is necessary for the trafficking of Innexin proteins to specific subcellular regions (Palumbos et al., 2021), it is enticing to speculate that Neurobeachin may be the cell biological link between cAMP signaling and the compartmentalized trafficking of electrical synapse components. Overall, these overlapping pieces of evidence imply that neurons across many organisms may share mechanisms in building their electrical synapses.

As Neurobeachin is necessary for both electrical and chemical synapse development, an essential question is whether this protein uses similar or distinct mechanisms to regulate these molecularly diverse structures. Does Neurobeachin drive specific subcellular targeting of chemical postsynaptic proteins to the synapse? Previous work shows that Neurobeachin co-localizes with chemical synapse scaffolding molecules like SAP102 along dendrites as well as at the synapse (Lauks et al., 2012). Upon Neurobeachin loss, chemical synapse receptors do not localize to the cell surface, but instead accumulate within the cell soma (Nair et al., 2013). Yet whether Neurobeachin functions to restrict postsynaptic chemical synapse proteins to the dendrite has not been examined. Altogether, this work illuminates a biochemical and cell biological mechanism at the nexus of balancing the electrical and chemical synaptogenesis that occurs during early neural circuit wiring and opens a window for future investigations underlying these fundamental processes.

Materials and Methods

Zebrafish

Zebrafish (*Danio rerio*) were bred and maintained with approval from the Institutional Animal Care and Use Committee (IACUC AUP 21-42) within the University of Oregon fish facility. Fish were kept at 28°C on a 14 hr on and 10 hr off light cycle and the developmental timepoints used originated from standard developmental staging (Kimmel et al., 1995). Animals were housed in groups according to genotype with a limit of 30 animals per tank. All fish for this project originated from the ABC background and most fish had the enhancer trap transgene *zf206Et (M/CoLo:GFP)* in the background, which labels the Mauthner and CoLo neurons with GFP (Satou et al., 2009), unless otherwise noted. Mutant lines were genotyped for all experiments, unless otherwise noted. At this stage of development, zebrafish sex is not yet determined (Wilson et al., 2014).

Table of zebrafish lines

Strain, strain background (*Danio rerio*)	*M/CoLo:GFP*	*zf206Et*
Strain, strain background (*Danio rerio*)	*tjp1b*$^{\Delta 16bp}$	*fh1370*
Strain, strain background (*Danio rerio*)	*gjd1a* $^{\Delta 8bp}$	*fh436*
Strain, strain background (*Danio rerio*)	*V5-tjp1b*	*b1406*
Strain, strain background (*Danio rerio*)	*nbeaa*	*fh364*
Strain, strain background (*Danio rerio*)	*Cx34.1oxGFP*	*AE37*

Generation of Cx34.1-oxGFP fish

To generate the fish in which Cx34.1 is tagged with a fluorescent protein, Cx34.1 was tagged with oxGFP, which is optimized for use in oxidizing environments and biological membranes (Costantini et al., 2015). A Cx34.1 coding region expression plasmid was made using zebrafish genomic bac clone CH211-87N9. The fluorescent protein coding region was inserted into the CT of the connexin at a site (21 aa before end of the CT) that was previously found not to disrupt regulation of coupling by connexin phosphorylation and not to block the C-terminal PDZ-domain interaction motif (Wang et al., 2015). Promoter elements of the connexin gene were derived from the same bac clone. The transgene construct also includes a mCherry cardiac reporter for ease of identification in injected embryos *(further details included in supplementary materials)*.

The transgenic fish (AE 37) was generated at the Zebrafish Core of the Albert Einstein College of Medicine using the Tol2 transposon system. The expression of the transgene at the expected synaptic sites at transgenic animals was validated using double-labeling with anti Cx34.1 and anti GFP, and electrical transmission was found to be indistinguishable from that of WT fish during electrophysiological recordings.

Cas9-mediated genome engineering of Cx35.5-V5 crispants

To generate fish at which endogenous Cx35.5 is tagged with V5 epitope tag, a single guide RNA (sgRNA) targeting exon 2 of the endogenous *gjd2a* coding sequence was designed using the CRISPRscan algorithm (Moreno-Mateos et al., 2015) and synthesized as previously described (Shah et al., 2015). The sgRNA was generated using the T7 megascript kit (ThermoFisher, AMB13345). The *gjd2a*-V5 single stranded donor oligo (ssODN) was designed to repair into the endogenous *gjd2a* locus 57 bp prior to the stop codon and was synthesized complementary to the coding strand. The ssODN contained 60 bp and 40 bp homology arms, respectively, flanked by a 5x glycine linker, with a V5 epitope tag in the center. Upon correct repair, the inserted sequence was designed to disrupt the endogenous sgRNA recognition site to prevent further double stranded breaks after repair. Injection mixes were prepared in a pH 7.5 buffer solution of 300 mM KCl and 4 mM HEPES and contained a final concentration of 200 pg/nL ssODN, 200 pg/nL gRNA, and 1600 pg/nL Cas9 protein (IDT, 1081058). Injection mixes were incubated at 37 °C for 5 min immediately prior to injection to promote formation of the Cas9 and sgRNA complex. Finally, 1 nL of solution was injected into M/CoLo:GFP (zf206Et) embryos at the one-cell stage. F0 crispants were used for analysis and signal verified by co-immunostaining with V5 and Cx35.5 antibody labeling.

Cell culture

HEK293T/17 verified cells were purchased from ATCC (CRL-11268; STR profile, amelogenin: X). Cells were passaged and maintained in Dulbecco's Modified Eagle's Medium (DMEM, ATCC) plus 10% fetal bovine serum (FBS, Gibco) at 37°C in a humidified incubator in the presence of 5% CO_2. Low passage aliquots were cryopreserved in liquid nitrogen according to manufacturer’s instructions. Cells from

each thawed cryovial were monitored for mycoplasma contamination using the Universal Mycoplasma Detection Kit (ATCC, 30–1012K).

Immunohistochemistry and confocal imaging

Anesthetized, 5 days post fertilization (dpf) larvae were fixed for 4 hr in 2% trichloroacetic acid in PBS, or for 1 hr in 4% PFA. Fixed tissue was washed in PBS + 0.5% Triton X-100, followed by standard blocking and antibody incubations. Primary antibody mixes included combinations of the following: rabbit anti-Cx35.5 (Fred Hutch Antibody Technology Facility, clone 12H5, 1:200), mouse IgG2A anti-Cx34.1 (Fred Hutch Antibody Technology Facility, clone 5C10A, 1:200), mouse IgG1 anti-ZO1 (Invitrogen, 33–9100, 1:350), mouse IgG2a anti-V5 peptide (Invitrogen, R960-25, 1:500), rabbit anti-Neurobeachin (Invitrogen, PA5-58903, 1:100), mouse anti-GM130, BD Biosciences, 1:100), mouse anti-RMO44** Neurofilament-M (Invitrogen, 13-0500, 1:50), and chicken anti-GFP (abcam, ab13970, 1:500) All secondary antibodies were raised in goat (Invitrogen, conjugated with Alexa-405,–488, −555, or −633 fluorophores, 1:500). Tissue was then cleared stepwise in a 25%, 50%, 75% glycerol series, dissected, and mounted in ProLong Gold antifade reagent (ThermoFisher, P36930). Images were acquired on a Leica SP8 Confocal using a 405-diode laser and a white light laser set to 499, 553/554/557 (consistent within experiments), and 631 nm, depending on the fluorescent dye imaged. Each laser line's data was collected sequentially using custom detection filters based on the dye. Quantitative images of the Club Endings (CEs) and M/CoLo transplants were collected using a 63x, 1.40 numerical aperture (NA) oil immersion lens, and other images of M/Colo synapses were collected using a 40x, 1.20 NA water immersion lens. For each set of images, the optimal optical section thickness was used as calculated by the Leica software based on the pinhole, emission wavelengths and NA of the lens. Within each experiment where fluorescence intensity was to be quantified, all animals (including 5 or more wildtype controls) were stained together with the same antibody mix, processed at the same time, and all confocal settings (laser power, scan speed, gain, offset, objective, and zoom) were identical. Multiple animals per genotype were analyzed to account for biological

variation. To account for technical variation, fluorescence intensity values for each region of each animal were an average across multiple synapses.

Cell transfection and immunoprecipitation

Full-length Cx34.1 and full-length Cx35.5 were cloned into the pCMV expression vector. Full-length ZO1b was cloned into the pCMV expression vector with a COOH-terminal 8xHIS tag. N-terminal and C-terminal Neurobeachin constructs were cloned into the pCMV expression vector with an mVenus tag. Low passage HEK293T/17 cells were seeded 24 hr prior to transfection (1×10^6 cells/well of a six-well dish), and the indicated plasmids were co-transfected using Lipofectamine 3000 (Invitrogen) following the manufacturer's instructions. Cells were collected 24 hr post-transfection and lysed in 500 mL solubilization buffer (50 mM Tris [pH7.4], 100 mM NaCl, 5 mM EDTA, 1.5 mM MgCl2, 1 mM DTT and 1% Triton X-100) plus a protease inhibitor cocktail (Pierce). Lysates were centrifuged at 20,000 x g for 30 min at 4°C, and equal amounts of extract were immunoprecipitated with 0.5 ug rabbit anti-GFP (Abcam, Ab290) overnight with rocking at 4°C. Immunocomplexes were captured with 40 µl prewashed Protein A/G agarose beads for 1 hr with rocking at 4°C. Beads were washed three times with lysis buffer, and bound proteins were boiled for 5 min in the presence of LDS-PAGE loading dye containing 200 mM DTT. Samples were resolved by SDS-PAGE using a 4–15% gradient gel and analyzed by Western blot using the following primary antibodies: chick anti-GFP (Abcam Ab13970), rabbit anti-Cx34.1 3A4-conjugated-800LT, and rabbit anti-Cx35.5 12H5-conjugated-800LT, mouse IgG1 anti-ZO1 (Invitrogen, 33–9100, 1:350). Compatible near-infrared secondary antibodies were used for visualization with the Odyssey system (LI-COR). Conjugated antibodies were synthesized using IRDye® 800CW Protein Labeling Kit (LiCor, 928-38040).

Western blotting of fish brain homogenates

Brains from *wildtype and nbeaa*$^{-/-}$ euthanized adult fish (4–15 months old) were removed, snap frozen in liquid nitrogen and stored at −80C until use. Brains were homogenized in 300uL of HSE buffer (20 mM Hepes [pH7.5], 150 mM NaCl, 5 mM EDTA, 5 mM EGTA, and 1 mM DTT) plus a protease inhibitor cocktail using a glass

homogenizer. Detergent was added to the homogenate (final 2% octyl ß-D-glucopyranoside, Anatrace) and solubilized overnight with rocking at 4°C. Solubilized homogenate was cleared by centrifugation at 20,000 x g for 30 min at 4°C. Samples were boiled for 5 min in the presence of LDS-PAGE loading dye containing 200 mM DTT. Proteins were examined by western analysis using the following primary antibodies: mouse anti-ZO1, rabbit anti-Cx34.1 3A4-conjugated-800LT, rabbit anti-Cx35.5 12H5-conjugated-800LT, rabbit anti-beta tubulin (abcam, ab6046, 1:10,000). Compatible near-infrared secondary antibodies were used for visualization.

Blastula cell transplantation

Cell transplantation was performed at the high stage approximately 3.3 hr into zebrafish development using standard techniques (Kemp et al., 2009). Embryos were chemically de-chorionated with protease type XIV (Sigma Aldrich, 9036-06-0) prior to transplantation. Cells were transplanted using a 50 mm wide glass capillary needle attached to an oil hydraulic. For '*V5-ZO1b nbeaa+/+ or nbeaa-/-* into *wildtype*' transplants, cells from genotyped animals in the M/CoLo:GFP background were transplanted into non-transgenic *wildtype* hosts. For '*Cx34.1-GFP nbeaa+/+ or nbeaa-/-* into *wildtype*' transplants, cells from genotyped animals were transplanted into non-transgenic *wildtype* hosts. Approximately 20 cells were deposited ∼10–15 cell diameters away from the margin, with a single donor embryo supplying cells to 1-3 hosts. At 5 dpf, larvae were fixed in TCA, donor animals genotyped, host animals sorted due to the genotype of the donor, and processed for immunohistochemistry.

Analysis of confocal imaging

For fluorescence intensity quantitation, confocal images were processed and analyzed using FiJi (Schindelin et al., 2012) software. To quantify staining at M/Colo synapses, a standard region of interest (ROI) surrounding each M/CoLo site of contact was drawn, and the mean fluorescence intensity was measured. For the quantification of staining at the club endings, confocal z-stacks of the Mauthner soma and lateral dendrite were cropped to 200 x 200 pixels centered around the lateral dendritic bifurcation. A FIJI-script was generated to clear the outside of the Mauthner cell, and a standard threshold

was set within each experiment to remove background staining. The image was then transformed into a max intensity projection, synapses thresholded to WT, and the integrated density of each stain within the club ending synapses was extracted. Standard deviations and errors were computed using Prism (GraphPad) or Excel (Microsoft) software. Figure images were created using FiJi, Photoshop (Adobe), and Illustrator (Adobe). Statistical analyses were performed using Prism (GraphPad). For all experiments unless otherwise listed in the figure legend, values were normalized to *wildtype* control animals, and n represented the number of fish used.

Acknowledgements: We would like to thank and acknowledge the Zebrafish facility at the University of Oregon who have given our fish the best possible care, especially through the challenges of the global pandemic. We would also like to thank and acknowledge Ali Eggling and Angela Loczi-Storm for contributions to data quantification while pursuing their undergraduate educations. Finally, we would also like to thank the administrative staff at the University of Oregon Institute of Neuroscience.

Competing Interests: None to declare.

Funding:
NIH grants F32HD102182 to E.A.M., RF1MH120016 to A.E.P, J.O.B., and A.C.M., R21NS085772 to A.E.P. and J.O.B., R01DC011099 to A.E.P., R01EY012857 to J.O.B., R21NS117967 to A.C.M., and R01NS105758 to A.C.M..

References

Alcamí P, Pereda AE (2019) Beyond plasticity: the dynamic impact of electrical synapses on neural circuits. Nat Rev Neurosci.

Autenrieth K, Bendzunas NG, Bertinetti D, Herberg FW, Kennedy EJ (2016) Defining A-Kinase Anchoring Protein (AKAP) Specificity for Protein Kinase A Subunit RI (PKA-RI). Chembiochem 17:693 Available at: /pmc/articles/PMC4836982/ [Accessed January 28, 2022].

Bowling KM et al. (2017) Genomic diagnosis for children with intellectual disability

and/or developmental delay. Genome Med 9 Available at: /pmc/articles/PMC5448144/ [Accessed January 28, 2022].

Costantini LM, Baloban M, Markwardt ML, Rizzo M, Guo F, Verkhusha V V., Snapp EL (2015) A palette of fluorescent proteins optimized for diverse cellular environments. Nat Commun 2015 61 6:1–13 Available at: https://www.nature.com/articles/ncomms8670 [Accessed January 28, 2022].

Curti S, Hoge G, Nagy JI, Pereda AE (2012) Synergy between Electrical Coupling and Membrane Properties Promotes Strong Synchronization of Neurons of the Mesencephalic Trigeminal Nucleus. J Neurosci 32:4341–4359 Available at: https://www.jneurosci.org/content/32/13/4341 [Accessed January 28, 2022].

De Rubeis S et al. (2014) Synaptic, transcriptional and chromatin genes disrupted in autism. Nat 2014 5157526 515:209–215 Available at: https://www.nature.com/articles/nature13772 [Accessed January 28, 2022].

del Pino I, Paarmann I, Karas M, Kilimann MW, Betz H (2011) The trafficking proteins Vacuolar Protein Sorting 35 and Neurobeachin interact with the glycine receptor β-subunit. Biochem Biophys Res Commun 412:435–440.

Draguhn A, Traub RD, Schmitz D, Jefferys JGR (1998) Electrical coupling underlies high-frequency oscillations in the hippocampus in vitro. Nat 1998 3946689 394:189–192 Available at: https://www.nature.com/articles/BF28184 [Accessed January 28, 2022].

Easley-Neal C, Fierro J, Buchanan JA, Washbourne P (2013) Late Recruitment of Synapsin to Nascent Synapses Is Regulated by Cdk5. Cell Rep 3:1199–1212.

Farzana F, Zalm R, Chen N, Li KW, Grant SGN, Smit AB, Toonen RF, Verhage M (2016) Neurobeachin Regulates Glutamate- and GABA-Receptor Targeting to Synapses via Distinct Pathways. Mol Neurobiol 53:2112–2123 Available at: http://link.springer.com/10.1007/s12035-015-9164-8 [Accessed March 12, 2020].

Iossifov I et al. (2014) The contribution of de novo coding mutations to autism spectrum disorder. Nature.

Jabeen S, Thirumalai V (2018) The interplay between electrical and chemical synaptogenesis. J Neurophysiol 120:1914–1922.

Kemp HA, Carmany-Rampey A, Moens C (2009) Generating Chimeric Zebrafish

Embryos by Transplantation. JoVE (Journal Vis Exp 29:e1394 Available at: https://www.jove.com/v/1394/generating-chimeric-zebrafish-embryos-by-transplantation [Accessed January 28, 2022].

Kimmel CB, Ballard WW, Kimmel SR, Ullmann B, Schilling TF (1995) Stages of embryonic development of the zebrafish. Dev Dyn 203:253–310 Available at: https://onlinelibrary.wiley.com/doi/full/10.1002/aja.1002030302 [Accessed January 28, 2022].

Kimmel CB, Sessions SK, Kimmel RJ (1981) Morphogenesis and synaptogenesis of the zebrafish mauthner neuron. J Comp Neurol 198:101–120 Available at: https://onlinelibrary.wiley.com/doi/full/10.1002/cne.901980110 [Accessed January 28, 2022].

Lampe PD, Lau AF (2000) Regulation of Gap Junctions by Phosphorylation of Connexins. Arch Biochem Biophys 384:205–215.

Lasseigne AM, Echeverry FA, Ijaz S, Michel JC, Martin EA, Marsh AJ, Trujillo E, Marsden KC, Pereda AE, Miller AC (2021) Electrical synaptic transmission requires a postsynaptic scaffolding protein. Elife 10.

Lauks J, Klemmer P, Farzana F, Karupothula R, Zalm R, Cooke NE, Li KW, Smit AB, Toonen R, Verhage M (2012) Synapse Associated Protein 102 (SAP102) Binds the C-Terminal Part of the Scaffolding Protein Neurobeachin. PLoS One 7:e39420 Available at: https://journals.plos.org/plosone/article?id=10.1371/journal.pone.0039420 [Accessed January 28, 2022].

Liu KS, Fetcho JR (1999) Laser Ablations Reveal Functional Relationships of Segmental Hindbrain Neurons in Zebrafish. Neuron 23:325–335.

Maeder CI, Shen K, Hoogenraad CC (2014) Axon and dendritic trafficking. Curr Opin Neurobiol 27:165–170.

Marsh AJ, Michel JC, Adke AP, Heckman EL, Miller AC (2017a) Asymmetry of an Intracellular Scaffold at Vertebrate Electrical Synapses. Curr Biol 27:3561-3567.e4.

Marsh AJ, Michel JC, Adke AP, Heckman EL, Miller AC (2017b) Asymmetry of an Intracellular Scaffold at Vertebrate Electrical Synapses. Curr Biol.

Martin EA, Lasseigne AM, Miller AC (2020) Understanding the Molecular and Cell

Biological Mechanisms of Electrical Synapse Formation. Front Neuroanat 14:12.
Medrihan L, Rohlmann A, Fairless R, Andrae J, Döring M, Missler M, Zhang W, Kilimann MW (2009) Neurobeachin, a protein implicated in membrane protein traffic and autism, is required for the formation and functioning of central synapses. J Physiol 587:5095–5106 Available at: http://doi.wiley.com/10.1113/jphysiol.2009.178236 [Accessed March 12, 2020].
Mignogna ML, D'Adamo P (2017) Critical importance of RAB proteins for synaptic function. https://doi.org/101080/2154124820161277001 9:145–157 Available at: https://www.tandfonline.com/doi/abs/10.1080/21541248.2016.1277001 [Accessed January 28, 2022].
Miller AC, Pereda AE (2017) The electrical synapse: Molecular complexities at the gap and beyond. Dev Neurobiol.
Miller AC, Voelker LH, Shah AN, Moens CB (2015a) Neurobeachin is required postsynaptically for electrical and chemical synapse formation. Curr Biol.
Miller AC, Voelker LH, Shah AN, Moens CB (2015b) Neurobeachin is required postsynaptically for electrical and chemical synapse formation. Curr Biol 25:16–28.
Miller AC, Whitebirch AC, Shah AN, Marsden KC, Granato M, O'Brien J, Moens CB (2017a) A genetic basis for molecular asymmetry at vertebrate electrical synapses. Elife 6.
Miller AC, Whitebirch AC, Shah AN, Marsden KC, Granato M, O'Brien J, Moens CB (2017b) A genetic basis for molecular asymmetry at vertebrate electrical synapses. Elife.
Moreno-Mateos MA, Vejnar CE, Beaudoin JD, Fernandez JP, Mis EK, Khokha MK, Giraldez AJ (2015) CRISPRscan: designing highly efficient sgRNAs for CRISPR/Cas9 targeting in vivo. Nat Methods 12:982 Available at: /pmc/articles/PMC4589495/ [Accessed January 28, 2022].
Mulhern MS et al. (2018) NBEA: Developmental disease gene with early generalized epilepsy phenotypes. Ann Neurol 84:788–795 Available at: https://onlinelibrary.wiley.com/doi/abs/10.1002/ana.25350 [Accessed March 12, 2020].
Nagy JI, Pereda AE, Rash JE (2018) Electrical synapses in mammalian CNS: Past

eras, present focus and future directions. Biochim Biophys Acta - Biomembr.

Nair R, Lauks J, Jung SY, Cooke NE, de Wit H, Brose N, Kilimann MW, Verhage M, Rhee JS (2013) Neurobeachin regulates neurotransmitter receptor trafficking to synapses. J Cell Biol 200:61–80.

Niesmann K, Breuer D, Brockhaus J, Born G, Wolff I, Reissner C, Kilimann MW, Rohlmann A, Missler M (2011) Dendritic spine formation and synaptic function require neurobeachin. Nat Commun.

O'Rourke NA, Weiler NC, Micheva KD, Smith SJ (2012) Deep molecular diversity of mammalian synapses: why it matters and how to measure it. Nat Rev Neurosci 2012 136 13:365–379 Available at: https://www.nature.com/articles/nrn3170 [Accessed January 28, 2022].

Ou CY, Poon VY, Maeder CI, Watanabe S, Lehrman EK, Fu AKY, Park M, Fu WY, Jorgensen EM, Ip NY, Shen K (2010) Two Cyclin-Dependent Kinase Pathways Are Essential for Polarized Trafficking of Presynaptic Components. Cell 141:846–858.

Palumbos SD, Skelton R, McWhirter R, Mitchell A, Swann I, Heifner S, Von Stetina S, Miller DM (2021) cAMP controls a trafficking mechanism that maintains the neuron specificity and subcellular placement of electrical synapses. Dev Cell 56:3235-3249.e4.

Pereda AE (2014) Electrical synapses and their functional interactions with chemical synapses. Nat Rev Neurosci.

Rash JE, Curti S, Vanderpool KG, Kamasawa N, Nannapaneni S, Palacios-Prado N, Flores CE, Yasumura T, O'Brien J, Lynn BD, Bukauskas FF, Nagy JI, Pereda AE (2013) Molecular and functional asymmetry at a vertebrate electrical synapse. Neuron 79:957 Available at: /pmc/articles/PMC4020187/ [Accessed January 31, 2022].

Ravichandran Y, Goud B, Manneville JB (2020) The Golgi apparatus and cell polarity: Roles of the cytoskeleton, the Golgi matrix, and Golgi membranes. Curr Opin Cell Biol 62:104–113.

Roopun AK, Simonotto JD, Pierce ML, Jenkins A, Nicholson C, Schofield IS, Whittaker RG, Kaiser M, Whittington MA, Traub RD, Cunningham MO (2010) A nonsynaptic mechanism underlying interictal discharges in human epileptic neocortex. Proc Natl

Acad Sci U S A 107:338 Available at: /pmc/articles/PMC2806783/ [Accessed January 28, 2022].

Satou C, Kimura Y, Kohashi T, Horikawa K, Takeda H, Oda Y, Higashijima SI (2009) Functional Role of a Specialized Class of Spinal Commissural Inhibitory Neurons during Fast Escapes in Zebrafish. J Neurosci 29:6780–6793 Available at: https://www.jneurosci.org/content/29/21/6780 [Accessed January 28, 2022].

Schindelin J, Arganda-Carreras I, Frise E, Kaynig V, Longair M, Pietzsch T, Preibisch S, Rueden C, Saalfeld S, Schmid B, Tinevez JY, White DJ, Hartenstein V, Eliceiri K, Tomancak P, Cardona A (2012) Fiji - an Open Source platform for biological image analysis. Nat Methods 9:676–682 Available at: /pmc/articles/PMC3855844/ [Accessed January 28, 2022].

Shah AN, Davey CF, Whitebirch AC, Miller AC, Moens CB (2015) Rapid reverse genetic screening using CRISPR in zebrafish. Nat Methods 12:535–540.

Sillar KT (2009) Mauthner cells. Curr Biol 19:R353–R355 Available at: http://www.cell.com/article/S0960982209007325/fulltext [Accessed January 28, 2022].

Simon A, Traub RD, Vladimirov N, Jenkins A, Nicholson C, Whittaker RG, Schofield I, Clowry GJ, Cunningham MO, Whittington MA (2014) Gap junction networks can generate both ripple-like and fast ripple-like oscillations. Eur J Neurosci 39:46–60 Available at: https://pubmed.ncbi.nlm.nih.gov/24118191/ [Accessed January 28, 2022].

Südhof TC (2012) The presynaptic active zone. Neuron 75:11–25.

Vervaeke K, Lorincz A, Nusser Z, Silver RA (2012) Gap junctions compensate for sublinear dendritic integration in an inhibitory network. Science (80-) 335:1624–1628 Available at: https://www.science.org/doi/abs/10.1126/science.1215101 [Accessed January 28, 2022].

Wang HY, Lin YP, Mitchell CK, Ram S, O'Brien J (2015) Two-color fluorescent analysis of connexin 36 turnover: Relationship to functional plasticity. J Cell Sci 128:3888–3897.

Wang X, Herberg FW, Laue MM, Wullner C, Hu B, Petrasch-Parwez E, Kilimann MW (2000) Neurobeachin: A protein kinase A-anchoring, beige/Chediak-Higashi protein

homolog implicated in neuronal membrane traffic. J Neurosci 20:8551–8565.

Wilson CA, High SK, McCluskey BM, Amores A, Yan YL, Titus TA, Anderson JL, Batzel P, Carvan MJ, Schartl M, Postlethwait JH (2014) Wild sex in zebrafish: Loss of the natural sex determinant in domesticated strains. Genetics 198:1291–1308 Available at: /pmc/articles/PMC4224167/ [Accessed January 28, 2022].

Yadav S, Linstedt AD (2011) Golgi Positioning. Cold Spring Harb Perspect Biol 3:1–17 Available at: /pmc/articles/PMC3101843/ [Accessed January 28, 2022].

Yao C, Vanderpool KG, Delfiner M, Eddy V, Lucaci AG, Soto-Riveros C, Yasumura T, Rash JE, Pereda AE (2014) Electrical synaptic transmission in developing zebrafish: properties and molecular composition of gap junctions at a central auditory synapse. J Neurophysiol 112:2102–2113 Available at: https://www.physiology.org/doi/10.1152/jn.00397.2014 [Accessed March 13, 2020].

Figure 1

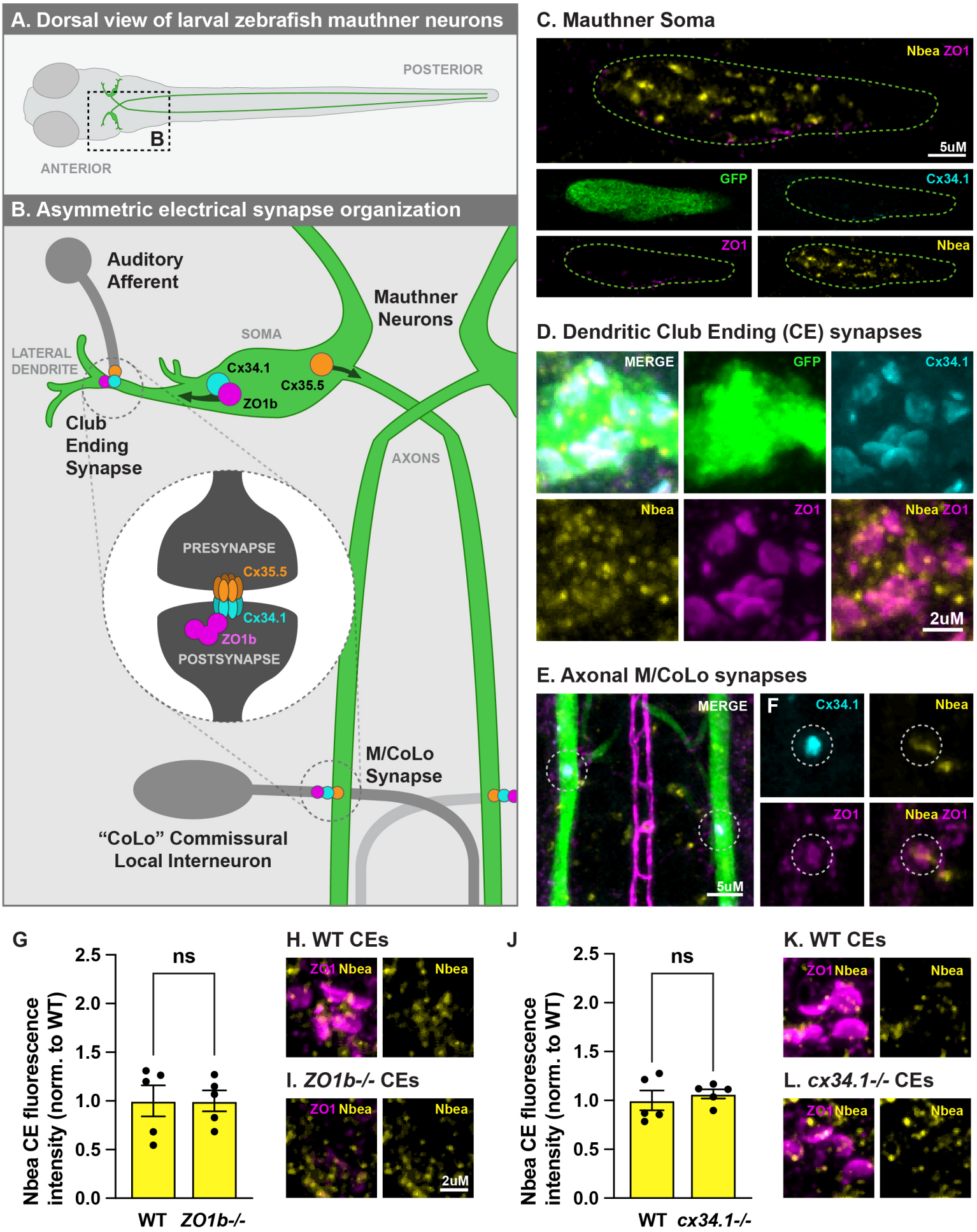
A. Dorsal view of larval zebrafish mauthner neurons
POSTERIOR
B
ANTERIOR
B. Asymmetric electrical synapse organization
Auditory Afferent
Mauthner Neurons
SOMA
LATERAL DENDRITE
Cx34.1
Cx35.5
ZO1b
Club Ending Synapse
AXONS
PRESYNAPSE
Cx35.5
Cx34.1
ZO1b
POSTSYNAPSE
M/CoLo Synapse
"CoLo" Commissural Local Interneuron
C. Mauthner Soma
Nbea ZO1
5uM
GFP
Cx34.1
ZO1
Nbea
D. Dendritic Club Ending (CE) synapses
MERGE
GFP
Cx34.1
Nbea
ZO1
Nbea ZO1
2uM
E. Axonal M/CoLo synapses
MERGE
5uM
F
Cx34.1
Nbea
ZO1
Nbea ZO1
G
ns
Nbea CE fluorescence intensity (norm. to WT)
2.5
2.0
1.5
1.0
0.5
0.0
WT
ZO1b-/-
H. WT CEs
ZO1 Nbea
Nbea
I. ZO1b-/- CEs
ZO1 Nbea
Nbea
2uM
J
ns
Nbea CE fluorescence intensity (norm. to WT)
2.5
2.0
1.5
1.0
0.5
0.0
WT
cx34.1-/-
K. WT CEs
ZO1 Nbea
Nbea
L. cx34.1-/- CEs
ZO1 Nbea
Nbea

Figure 1: Neurobeachin is expressed in the Mauthner circuit and localizes to the synapse independent of ZO1b or Cx proteins

(A) Dorsal view of the larval zebrafish illustrating location of the two Mauthner neurons (green). Boxed region indicated the region zoom shown in B. **(B)** Simplified illustration of the Mauthner circuit which identifies the synapses examined and the known protein localization of electrical synapse components Cx34.1 (cyan), Cx35.5 (orange), and ZO1b (magenta). The center dashed-circle diagram depicts the standard synapse organization for each Mauthner synapse which includes gap junction hemichannels composed of Cx35.5 in the presynapse, and Cx34.1 in the postsynapse where it binds scaffolding protein ZO1b. The top left dashed circle along the Mauthner lateral dendrite indicates a Club Ending (CE), which connects an auditory afferent to Mauthner. The bottom right dashed circle along the Mauthner axon indicates an M/CoLo synapse which connects Mauthner to Commissural Local (CoLo) interneurons. These axonal synapses are continued pairwise, in each segment of the fish moving down the spinal cord. Diagram shows Mauthner subcellular localization of postsynaptic proteins Cx34.1 and ZO1b to the CE synapses along the dendrite, and presynaptic Cx35.5 to the M/CoLo synapses in the axon. **(C-E)** Confocal images of Mauthner subcellular regions in 5-days-post-fertilization (dpf) *zf206Et*, transgenic *wildtype* zebrafish. Panels show staining for GFP labeling the Mauthner cell (green), Cx34.1 (cyan), Neurobeachin (yellow), ZO1 (magenta) at: **(C)** Mauthner cell soma, **(D)** dendritic CE synapses, and **(E)** axonal M/CoLo synapses. Images are maximum intensity projections. Green dashed outline in C represents the cell soma. White dashed outline in E represents the M/CoLo electrical synapse site. **(G-L)** Quantification of staining and representative confocal images of Mauthner CE synapses in 5dpf, *zf206Et*, transgenic zebrafish from *wildtype* (WT, **H,K**), *tjp1b/ZO1b*$^{-/-}$ mutant animals (**I**), and gjd1a/Cx34.1$^{-/-}$ mutant animals **(L)**. **(G)** Quantification of Neurobeachin fluorescence intensities at *wildtype* (WT) and *tjp1b/ZO1b*$^{-/-}$ (ZO1b-/-) CE normalized to WT. **(H,I)** Representative images of wildtype **(H)** and *tjp1b/ZO1b*$^{-/-}$ (Zo1b-/-) **(I)** CE synapses with markers as indicated. **(J)** Quantification of Neurobeachin fluorescence intensities at *wildtype* (WT) and *gjd1a/Cx34.1*$^{-/-}$ (Cx34.1-/-) CE synapses normalized to WT. **(K,L)** Representative images of wildtype **(K)** and *gjd1a/Cx34.1*$^{-/-}$ (Cx34.1-/-) **(L)** CE synapses with markers as

indicated. Circles in the bar graphs represent the normalized value of each individual animal (CE synapses from 2 dendrites per animal averaged to produce single value for each animal). For G-L, comparisons were made between genotyped WT and mutant sibs. *wildtype* (G and J) n = 5, *tjp1b/ZO1b*$^{-/-}$ n = 5, *gjd1a/Cx34.1*$^{-/-}$ n = 5. No significant difference found by unpaired t-test. Error bars are ± SEM. Scale bars are as indicated in graphic.

Supplementary Figure 1

A. *nbeaa-/-* Mauthner Soma

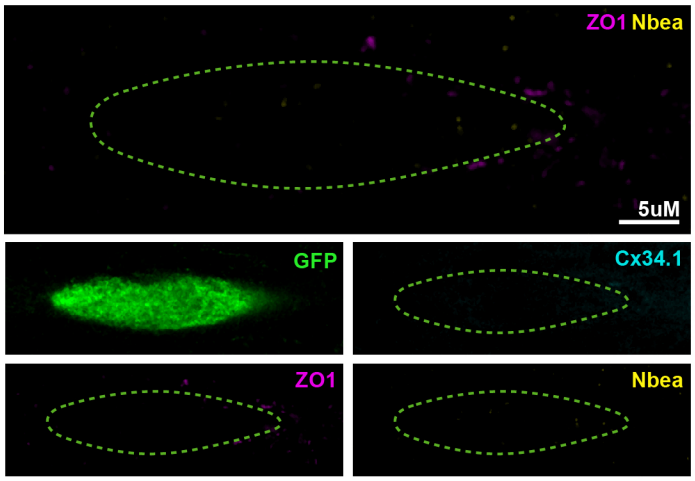

B. *nbeaa-/-* Dendritic CE synapses

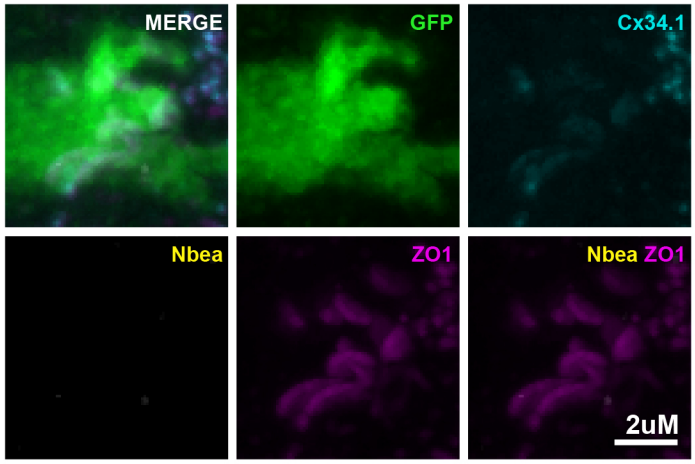

C. *nbeaa-/-* Axonal M/CoLo synapses

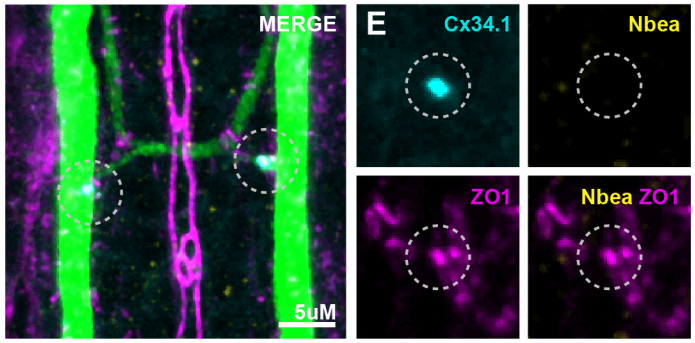

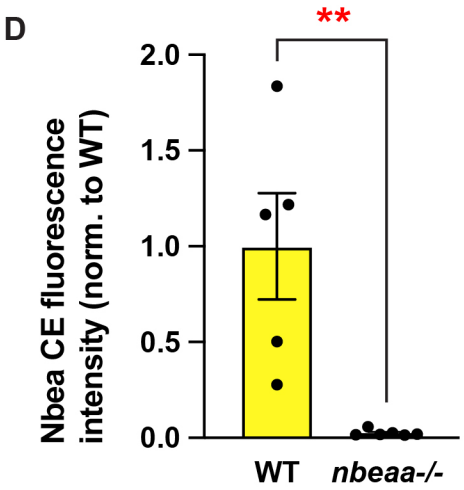

Supplementary Figure 1: Neurobeachin mutants show no Neurobeachin staining

(A-C) Confocal images of Mauthner subcellular regions in 5-days-post-fertilization (dpf) *zf206Et*, transgenic *nbeaa-/-* mutant zebrafish. Panels show staining for GFP labeling the Mauthner cell (green), Cx34.1 (cyan), Neurobeachin (yellow), ZO1 (magenta) at: **(A)** Mauthner cell soma, **(B)** dendritic CE synapses, and **(C)** axonal M/CoLo synapses. Images are maximum intensity projections. Green dashed outline in A represents the cell soma. White dashed outline in C represents the M/CoLo electrical synapse site. **(D)** Quantification of Neurobeachin fluorescence intensities at *wildtype* (WT) and *nbeaa* $^{-/-}$ CE synapses normalized to WT. For D, comparisons were made between genotyped WT and mutant sibs. Mean ± SEM are shown, n = 5, ** indicates $p < 0.01$ by Mann Whitney.

Figure 2

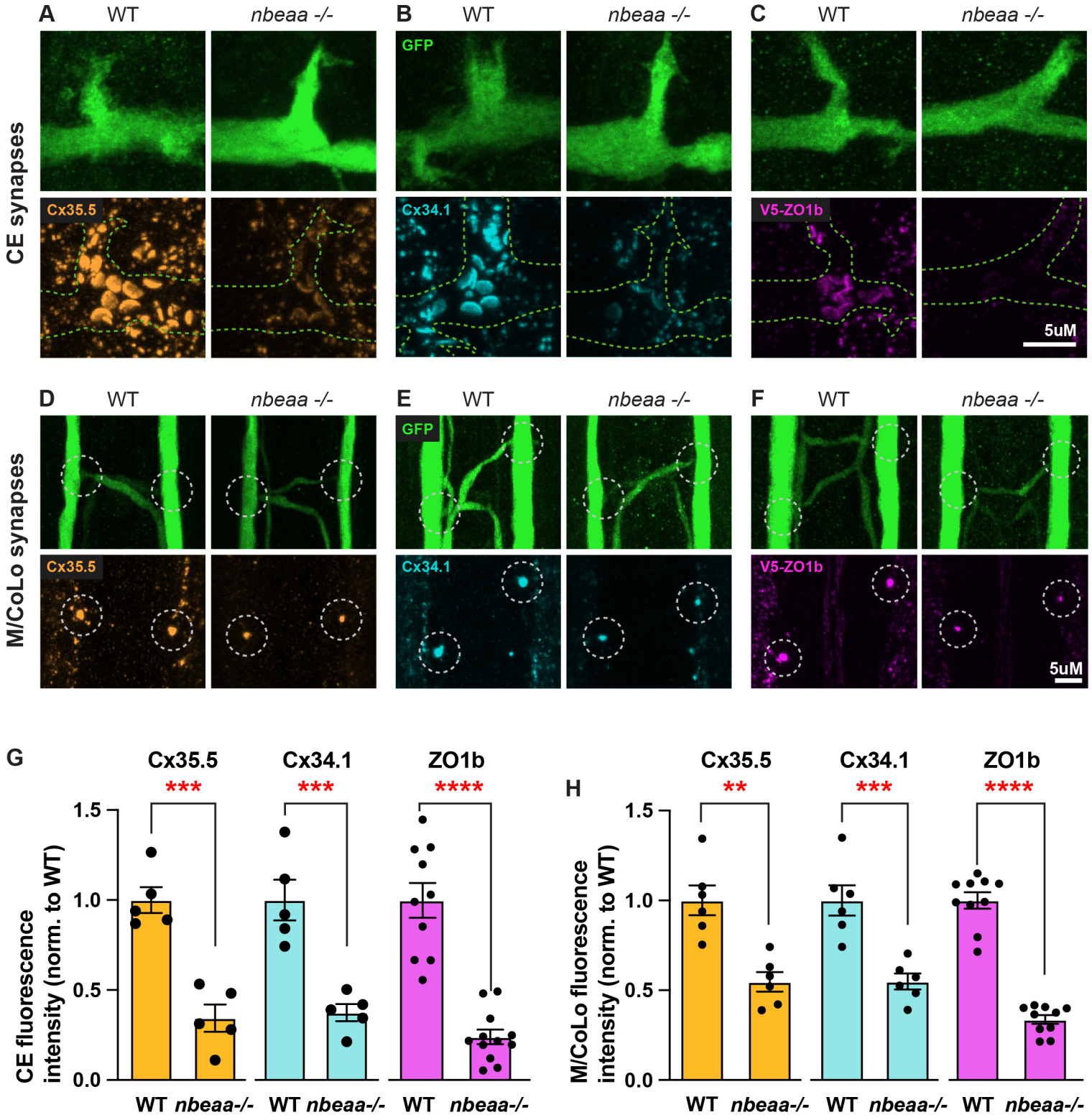
A
WT
nbeaa -/-
B
WT
nbeaa -/-
C
WT
nbeaa -/-
CE synapses
GFP
Cx35.5
Cx34.1
V5-ZO1b
5uM
D
WT
nbeaa -/-
E
WT
nbeaa -/-
F
WT
nbeaa -/-
M/CoLo synapses
GFP
Cx35.5
Cx34.1
V5-ZO1b
5uM
G
Cx35.5
Cx34.1
ZO1b
***
***
****
CE fluorescence intensity (norm. to WT)
1.5
1.0
0.5
0.0
WT
nbeaa-/-
WT
nbeaa-/-
WT
nbeaa-/-
H
Cx35.5
Cx34.1
ZO1b
**
***
****
M/CoLo fluorescence intensity (norm. to WT)
1.5
1.0
0.5
0.0
WT
nbeaa-/-
WT
nbeaa-/-
WT
nbeaa-/-

Figure 2: Neurobeachin loss results in the similar reduction of pre- and post-synaptic electrical synapse proteins

(A-F) Confocal images of Mauthner synapses in 5 dpf *zf206Et*, transgenic *wildtype* or *nbeaa-/-* zebrafish. Panels show staining for GFP labeling the Mauthner cell (green), Cx34.1 (cyan), Cx35.5 (orange), ZO1 (magenta) at: **(A-C)** CE synapses, and **(D-F)** M/CoLo synapses. (A-C) Dashed lines in bottom image indicate outline of Mauthner cell shown in top image. (D-F) Dashed circles identify electrical synapses. **(G)** Quantification of indicated electrical synapse protein fluorescence intensities at CE synapses (Cx34.1, Cx35.5, and ZO1) in *wildtype* (WT) and *nbeaa*$^{-/-}$ normalized to WT. **(H)** Quantification of indicated electrical synapse protein fluorescence intensities at M/CoLo synapses (Cx34.1, Cx35.5, and ZO1) in *wildtype* (WT) and *nbeaa*$^{-/-}$ normalized to WT. Mean ± SEM are shown, All comparisons were made between genotyped WT and mutant siblings. For graph in G, n = 5, 5, 5, 5, 10, and 12 fish, respectively, with the fluorescence intensities normalized to wildtype, and two Mauthner neurons analyzed per fish and averaged to represent a single value for each fish. The average intensity value of the two neurons is the value represented for each fish. For graph in H, n = 6, 6, 6, 6, 10, and 10 fish, respectively, with the fluorescence intensities normalized to WT, and 20-24 M/Colo synapses analyzed per fish. The average intensity value of all M/CoLo synapses is the value represented for each fish. ** indicates $p < 0.01$, *** indicates $p < 0.001$, **** indicates $p < 0.0001$ by unpaired t-test. Scale bars are as indicated.

Supplementary Figure 2

A

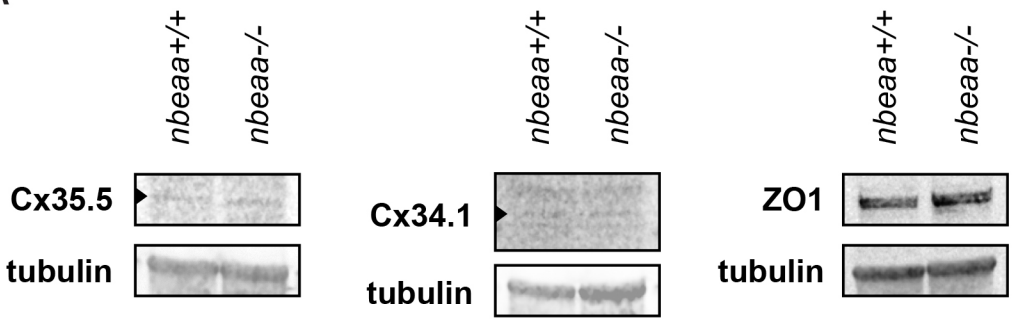

Supplementary Figure 2: Neurobeachin mutants show no loss of total Cx35.5, Cx34.1, or ZO1b protein

(**A**) Zebrafish brain extract from WT (*nbeaa+/+*, lane 1) or *nbeaa*$^{-/-}$ mutant (lane 2) animals blotted for Cx35.5, Cx34.1, and ZO1 proteins. As a loading control, blots were also tested for beta-tubulin. Results are representative of three independent experiments.

Figure 3

A Full length Neurobeachin:

mVenus-tagged N-terminal Neurobeachin:

mVenus-tagged C-terminal Neurobeachin:

B Transfection:

ZO1b	+	+
GFP	+	-
mVenus-C-term Neurobeachin	-	+

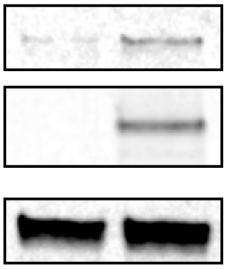

IP with anti-GFP

ZO1b

mVenus-C-term Neurobeachin

5% Input ZO1b

C Transfection:

Cx35.5	+	+
mVenus-**N**-term Neurobeachin	+	-
mVenus-**C**-term Neurobeachin	-	+

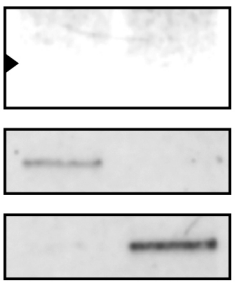

IP with anti-GFP

Cx35.5

mVenus-**N**-term Neurobeachin

mVenus-**C**-term Neurobeachin

5% Input Cx35.5

D Transfection:

Cx34.1	+	+
mVenus-**N**-term Neurobeachin	+	-
mVenus-**C**-term Neurobeachin	-	+

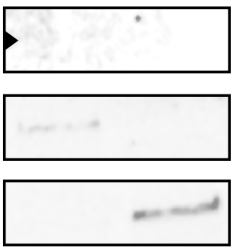

IP with anti-GFP

Cx34.1

mVenus-**N**-term Neurobeachin

mVenus-**C**-term Neurobeachin

5% Input Cx34.1

Figure 3: Neurobeachin binds postsynaptic electrical synapse scaffold ZO1b, but not Cx35.5 or Cx34.1

(A) Outline of Neurobeachin indicating domains included in mVenus-tagged N- and C-terminal Neurobeachin fragments. **(B)** HEK293T/17 cells were transfected with plasmids to express ZO1b and either GFP (lane 1), or mVenus-tagged C-terminal-Neurobeachin (lane 2). Lysates were immunoprecipitated with anti-GFP antibody and analyzed by immunoblot for the presence of ZO1b using ZO1 antibody (upper), or mVenus-tagged C-terminal Neurobeachin using GFP antibody (middle). Total extracts (bottom, 5% input) were blotted for ZO1b to demonstrate equivalent expression and uniform antibody recognition of expressed proteins. **(C)** HEK293T/17 cells were transfected with plasmids to express Cx35.5 and either mVenus-tagged N-terminal Neurobeachin (lane 1), or mVenus-tagged C-terminal-Neurobeachin (lane 2). Lysates were immunoprecipitated with anti-GFP antibody and analyzed by immunoblot for the presence of Cx35.5 using a specific Cx35.5 antibody (upper, note signal present from the antibody heavy chains above, but not at the Cx35.5 band site), mVenus-tagged N-terminal Neurobeachin using GFP antibody (middle), or mVenus-tagged C-terminal Neurobeachin using GFP antibody (lower). Total extracts (bottom, 5% input) were blotted for Cx35.5 to demonstrate expression. **(D)** HEK293T/17 cells were transfected with plasmids to express Cx34.1and either mVenus-tagged N-terminal Neurobeachin (lane 1), or mVenus-tagged C-terminal-Neurobeachin (lane 2). Lysates were immunoprecipitated with anti-GFP antibody and analyzed by immunoblot for the presence of Cx34.1 using a specific Cx34.1 antibody (upper, note signal present from the antibody heavy chains above, but not at the Cx34.1 band site), mVenus-tagged N-terminal Neurobeachin using GFP antibody (middle), or mVenus-tagged C-terminal Neurobeachin using GFP antibody (lower). Total extracts (bottom, 5% input) were blotted for Cx34.1 to demonstrate expression.

Figure 4

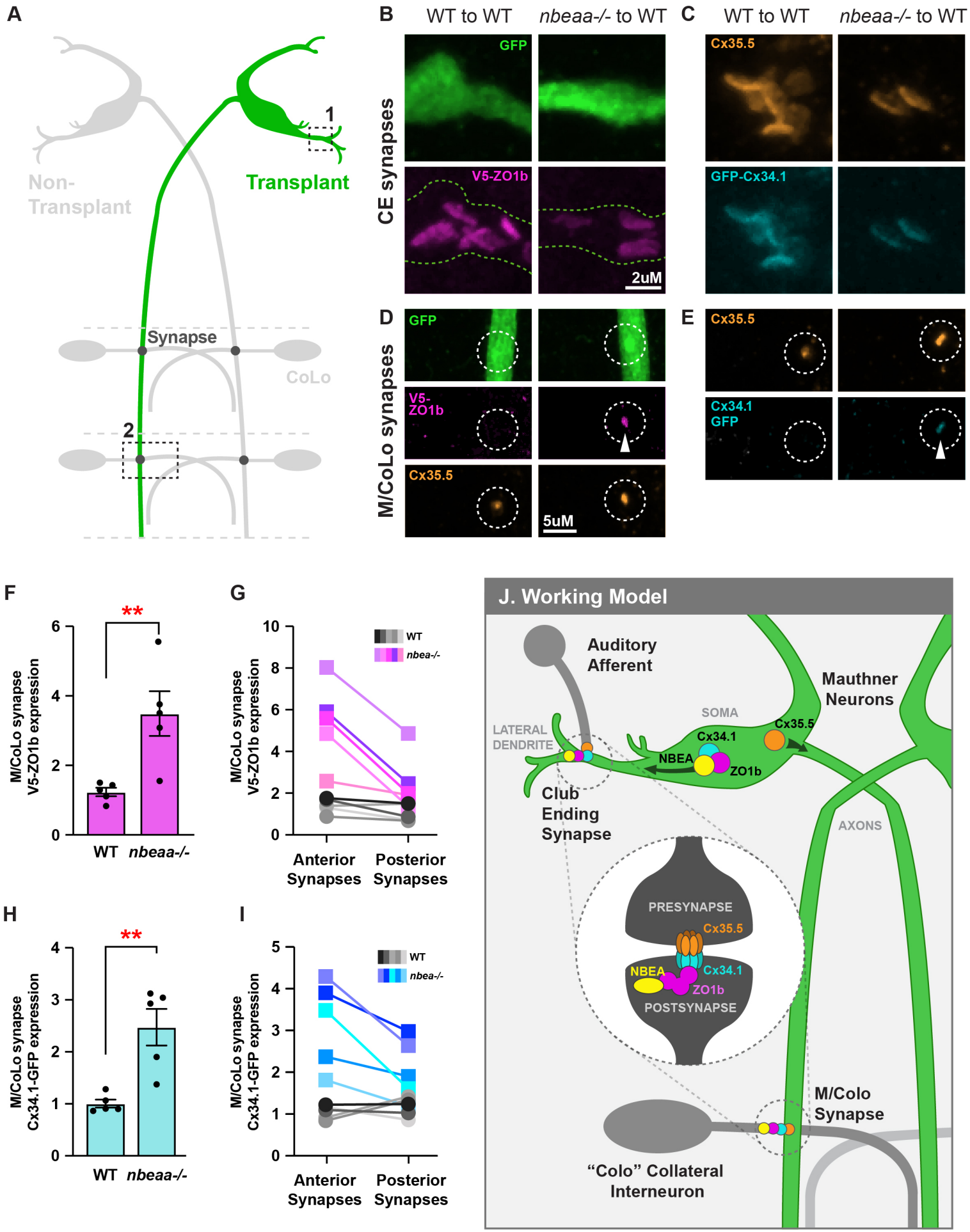
A
Non-Transplant
Transplant
1
Synapse
CoLo
2
B
WT to WT
nbeaa-/- to WT
CE synapses
GFP
V5-ZO1b
2uM
C
WT to WT
nbeaa-/- to WT
Cx35.5
GFP-Cx34.1
D
M/CoLo synapses
GFP
V5-ZO1b
Cx35.5
5uM
E
Cx35.5
Cx34.1
GFP
F
**
M/CoLo synapse V5-ZO1b expression
WT
nbeaa-/-
G
WT
nbea-/-
M/CoLo synapse V5-ZO1b expression
Anterior Synapses
Posterior Synapses
H
**
M/CoLo synapse Cx34.1-GFP expression
WT
nbeaa-/-
I
WT
nbea-/-
M/CoLo synapse Cx34.1-GFP expression
Anterior Synapses
Posterior Synapses
J. Working Model
Auditory Afferent
Mauthner Neurons
SOMA
LATERAL DENDRITE
Cx35.5
Cx34.1
NBEA
ZO1b
Club Ending Synapse
AXONS
PRESYNAPSE
Cx35.5
NBEA
Cx34.1
ZO1b
POSTSYNAPSE
M/Colo Synapse
"Colo" Collateral Interneuron

Figure 4: Neurobeachin is required for the proper synaptic compartmentalization of ZO1b and Cx34.1

(A) Diagram illustrating 5dpf Mauthner circuit after transplantation of a single Mauthner neuron (green). Boxed outline 1: Location of CE synapses shown by representational confocal images in D and E. Boxed outline 2: Location of M/Colo synapses shown by representative confocal images in F and G. **(B)** Confocal images of transplanted Mauthner CE synapses identified by GFP-positive Mauthner neuron. Top images represent transplanted WT Mauthner neuron in an WT host (left), and a transplanted nbeaa-/- Mauthner neuron in an WT host (right). Bottom images show V5 staining for V5-ZO1b for transplanted WT Mauthner neuron in an WT host (left), and a transplanted nbeaa-/- Mauthner neuron in an WT host (right). Outline of Mauthner neuron shown by green dashed line in bottom images. **(C)** Confocal images of transplanted Mauthner CE synapses identified by Cx34.1-GFP-positive CE synapses. Top images represent Cx35.5 staining in transplanted WT Mauthner neuron in an WT host (left), and a transplanted nbeaa-/- Mauthner neuron in an WT host (right). Bottom images show Cx34.1-GFP labeling of CE synapses in transplanted WT Mauthner neuron in an WT host (left), and a transplanted nbeaa-/- Mauthner neuron in an WT host (right). **(D)** Confocal images of transplanted Mauthner M/CoLo synapses identified by GFP-positive Mauthner axon. Righthand images represent transplanted WT Mauthner axon in an otherwise WT fish, lefthand images represent a transplanted nbeaa-/- Mauthner neuron in an otherwise WT fish. Top images show GFP labeling of Mauthner axon, middle images show staining for V5-tagged ZO1b, and bottom images show staining for Cx35.5. White arrow shows aberrant presynaptic V5-ZO1b. **(E)** Confocal images of transplanted Mauthner M/CoLo synapses identified by Cx34.1-GFP-positive CE synapses (shown in C). Lefthand images represent transplanted WT Mauthner axon in an otherwise WT fish, righthand images represent a transplanted nbeaa-/- Mauthner neuron in an otherwise WT fish. Top images show Cx35.5 labeling of M/Colo synapses, bottom images show staining for Cx34.1-GFP staining of M/CoLo synapses. White arrow shows aberrant presynaptic Cx34.1. **(F)** Quantification of V5-ZO1b labeling at M/Colo synapses in wildtype Mauthner neuron transplants (WT) and in nbeaa-/- Mauthner neuron transplants shown in D. To generate fluorescence intensity,

transplanted neuron V5-ZO1b fluorescence intensity at the synapse was normalized to non-transplanted V5-ZO1b expression at the synapse as well as synapse size. **(G)** V5-ZO1b fluorescence intensity (as calculated in F) at anterior versus posterior M/Colo synapses in wildtype Mauthner neuron transplants (WT) and in nbeaa-/- Mauthner neuron transplants. **(H)** Quantification of Cx34.1-GFP labeling at M/Colo synapses in wildtype Mauthner neuron transplants (WT) and in nbeaa-/- Mauthner neuron transplants shown in E. To generate fluorescence intensity, transplanted neuron Cx34.1-GFP fluorescence intensity was normalized to non-transplanted Cx34.1-GFP expression as well as synapse size. **(I)** Cx34.1-GFP fluorescence intensity (as calculated in H) at anterior versus posterior M/Colo synapses in wildtype Mauthner neuron transplants (WT) and in nbeaa-/- Mauthner neuron transplants. **(J)** Diagram showing proposed Neurobeachin (yellow) roles in regulating Mauthner neuron electrical synapse proteins. Mean ± SEM are shown, All comparisons were made between genotyped WT and mutant siblings. For (H,I) *wt,* n = 5, *nbeaa*$^{-/-}$, n = 5. For (J,K) *wt,* n = 5, *nbeaa*$^{-/-}$, n = 5. ** indicates $p < 0.01$ by unpaired t-test. Scale bars are as indicated.

Supplementary Figure 4

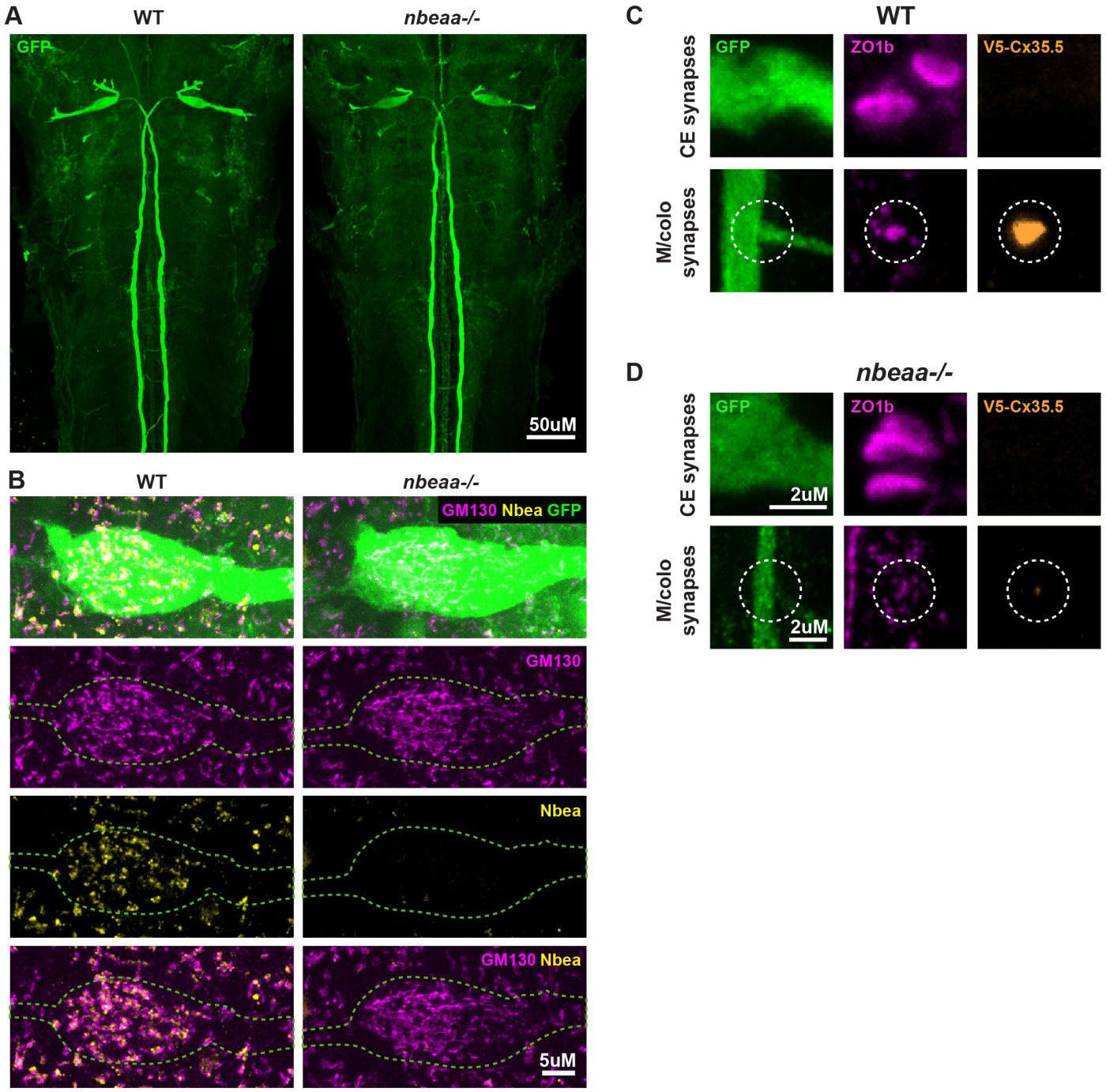

Supplementary Figure 4: Neuronal polarity appears normal in *nbeaa-/-* fish

(A) Confocal images of *zf206Et*, transgenic zebrafish from *wildtype* (WT) and *nbeaa*$^{-/-}$ mutant animals showing Mauthner somas, dendrites, and axons labeled with GFP (green). **(B)** Confocal images of *zf206Et*, transgenic zebrafish from *wildtype* (WT, left) and *nbeaa*$^{-/-}$ mutant animals (right) showing Mauthner cell somas immunostained for GM130 (magenta), Neurobeachin (yellow), and GFP (green). **(C,D)** Confocal images of *zf206Et*, transgenic zebrafish from (C) *wildtype* (WT) and (D) *nbeaa*$^{-/-}$ mutant 5 days-post-fertilization larvae grown from injected Cx35.5-V5 embryos. Top images show CE synapses. Bottom images identify M/Colo synapses with successful labeling of Cx35.5 with V5, synapse area outline with white dotted circle. Left images show GFP labeling of the Mauthner neuron, middle images show ZO1b staining to recognize synapse structures, right images show Cx35.5-V5 signal. Scale bars are as indicated.